Chasing sub-micrometer axial resolution in Visible Optical Coherence Tomography

Gianni Nteroli*, Adrian Bradu and Adrian Podoleanu

Applied Optics Group, School of Physical Sciences, University of Kent, Canterbury, UK
*E-mail: gn86@kent.ac.uk

Abstract: Optical Coherence Tomography instruments can provide images of ultrahigh, depth dependent axial resolution. Here we demonstrate an instrument employing visible light, enhanced by the Master-Slave technique, which deliver nearly constant axial resolution over the whole imaging range.

Keywords: visible light, optical coherence tomography, imaging, ultrahigh resolution

1. Introduction

Visible Optical Coherence Tomography (VIS-OCT) is an emerging imaging technique that can provide ultrahigh axial resolution of biological tissues. By using lower wavelengths than the conventional OCT imaging instruments and employing broadband optical sources such as supercontinuum lasers, resolutions of typical 1-3 μm in tissue were demonstrated [1-2]. The reported axial resolutions are however referring to measurements performed for very shallow depths (optical path differences (OPDs) between the arms of the interferometer, close to zero. As mentioned in various reports [1-2] the value of the axial resolution is depth dependent. Typically, in NIR/IR OCT, a deterioration of the axial resolution of 1-2 μm over an imaging range of 1 mm does not have a tremendous effect on the sharpness of the image however, in VIS-OCT, doubling the axial resolution can affect the outcomes of the measurements greatly. Although noticed in various research papers, no rigorous study on mitigating the deterioration of the axial resolution with depth has been reported so far. In this paper, we demonstrate a VIS-OCT imaging instrument enhanced by the Complex Master-Slave technique [3-4] showing a nearly constant axial resolution of around 2.1 μm in air (1.5 μm in tissue) along the entire axial imaging range of the instrument.

2. Methodology, Results and Discussion

Light from a supercontinuum broadband light source (SuperK Extreme EXR-20, NKT Photonics), providing a broad spectrum of nearly 250 nm with a central wavelength at 600 nm, was directed towards the sample and reference arm of an interferometer using a directional coupler (30/70). In the sample arm, light was conveyed towards the object to be imaged using a pair of orthogonal galvo-scanners (6220H, Cambridge Technology) and an achromatic in-house developed scan lens. The optical power emitted by the source was altered in such a way that, only 120 μW reached the sample. Light back-scattered by the sample and reflected by a reference mirror interfered at the directional fibre coupler and was conveyed towards an in-house devised spectrometer. At the core of the spectrometer, a Basler Sprint SPL4096-140KM line camera was employed. To produce the plots/images shown in this abstract, all 4096 pixels of the camera were utilised and vertically binned, hence the size of each individual pixel was 10×20 μm, whereas camera was operated at 20 kHz. The axial range which can be targeted with our instrument, determined by the coherence length of waves after diffraction on the grating (532 nm CWL, 1800 l/mm, Wasatch Photonics) combined with the spectral capability of the camera in sampling the spectrum was 1.6 mm (in air). The sensitivity drop-off was measured by using a flat mirror as object and using the procedure described in [5].

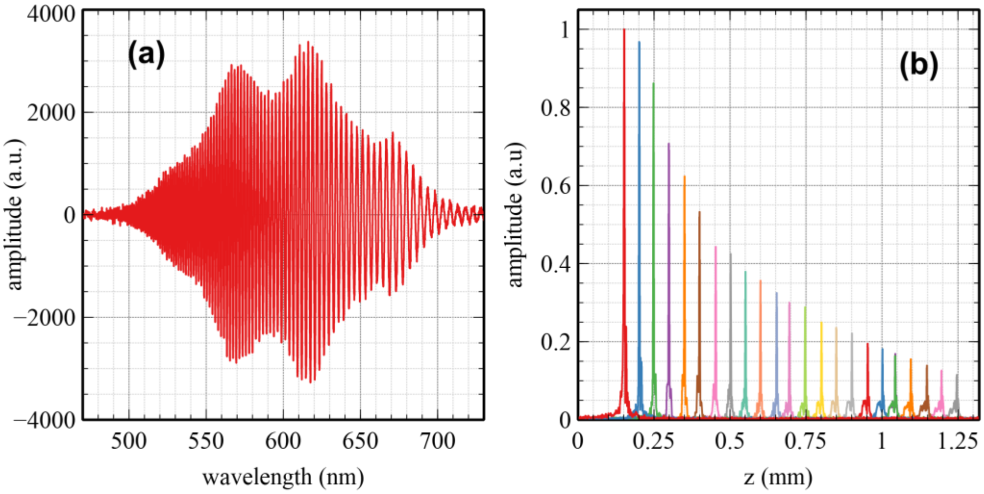

Figure 1 (a) Example of a channelled spectrum collected by the camera (to better observe the modulation, the channelled spectrum was high pass filtered before plotting). (b) Sensitivity drop-off of the instrument. All A-scans were normalised with respect of the maximum value of the A-scan produced when placing the sample mirror at z = 150 µm away from OPD = 0. The measured sensitivity of the instrument for z = 150 µm and 125 µWon the sample was 78 dB.

As it can be seen in Fig. 1(b), the sensitivity drops by around 10 dB over an axial range of 1 mm, which is slightly better than the values reported in literature (14-15 dB). The full-width-at-half-maximum axial resolution of each A-scan peak shown in Fig. 1(b) was measured. In Fig. 2(a1-a3), for clarity, A-scans corresponding to various OPDs are shown (no data apodization) whereas their equivalent A-scans when a Hamming window was applied to the spectra are demonstrated in Figs. 2(b1-b3). As it can be seen for the 3 A-scans presented, the axial range is around 2.1 µm, however a little worsening of the resolution with depth could be observed (increase by ~ 5% at z = 1.2 mm with respect to z = 150 µm). This increase of the axial resolution is expected, being due to the limited number of pixels utilised. A large bandwidth per each camera pixel translates into a reduction of the dynamic coherence length of the interfering waves. A poor sampling of the channelled spectrum with a low number of camera pixels leads to an interpolation failure in conventional Fourier transform based OCT [6]. By using no interpolation, and perfectly compensating for unbalanced dispersion in the interferometer, our CMS based instrument performs better at depth than the conventional ones.

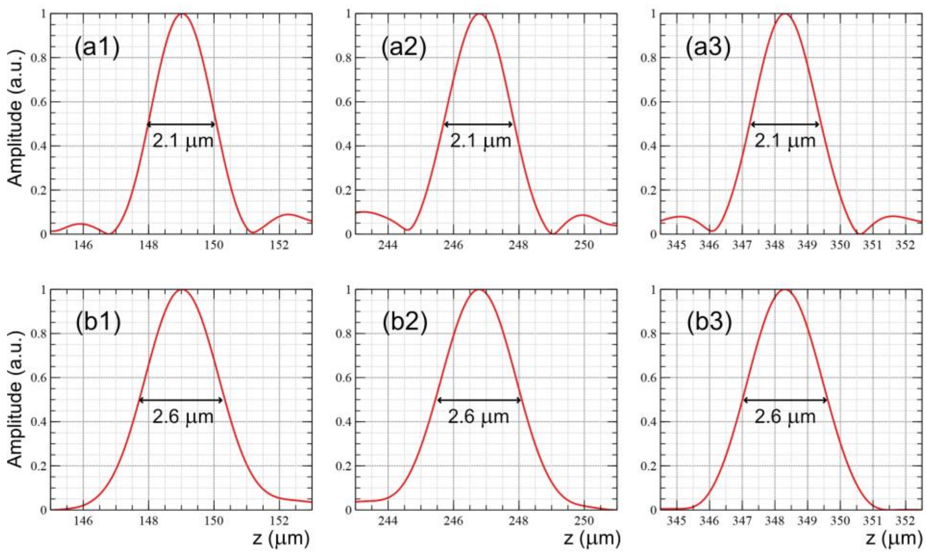

Figure 2 Examples of A-scans for various OPDs in the interferometer with no apodization of the spectra (a1-a3) and when a Hamming window was applied to the spectra (b1-b3).

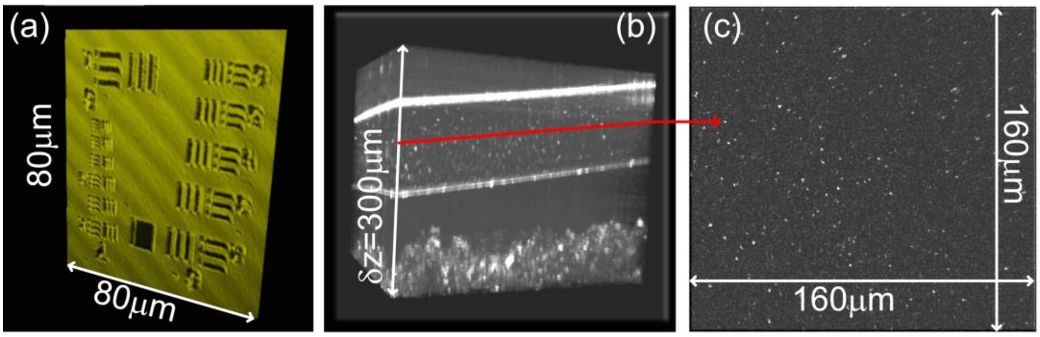

Figure 3 (a) 3D image of an USAF target showing that smallest future (group 7 element 6) is visible. **(b)** 3D image o fan IR card. **(c)** *En-face* view of the infrared card at the axial position shown by the red line.

In Fig. 3(a), a 3D image of an USAF target is demonstrated. As the smallest futures of this card are visible (group 7, element 6) are visible, the lateral resolution of our instrument is better than 2.19 μm (the theoretical value is 1.8 μm). In Fig. 3(b) a 3D image of an IR card is shown. The phosphor sensor area (bottom image) is below the coating layer. The fine borderline between the coating and the sensor is clearly visible. In Fig. 3(c) fine structures in the *en-face* view of the coating layer are shown. Additional details on the hardware employed, and the theoretical approach behind the VIS-OCT instrument we developed will be presented at the conference.

Acknowledgments

AP and AB acknowledge the support of BBSRC (BB/S016643/1) and GN and AP the support of the NIHR Biomedical Research Centre at the UCL Institute of Ophthalmology and Moorfields Eye Hospital.

References

[1] X. Shu, L. Beckhmann, and H. Zhang, "VIS OCT: a review", J. Biomed. Opt, **22**, p.121707 (2017).
[2] T. Zhang, et al, "Improving VIS OCT of the human retina with rapid spectral shaping and axial tracking", Biomed. Opt. Express **6**, p. 2918-2931 (2019).
[3] S. Rivet, et. al, "Complex master slave interferometry", Opt. Express 24, 2885-2904 (2016).
[4] A. Bradu et al, "Recovering distance information in spectral domain interferometry", Sci. Rep. **8**, p.15445 (2018).
[5] A. Bradu and A. Podoleanu, "Attenuation of mirror image and enhancement of the signal-to-noise ratio in a Talbot bands OCT system," J. Biomed. Opt. 16, 076010 (2011).
[6] Yun et al, "High-speed spectral-domain OCT at 1.3 μm wavelength," Opt. Express **11**, p.3598–3604 (2003).